The 9th European Congress on Computational Methods in Applied Sciences and Engineering
ECCOMAS Congress 2024
3–7 June 2024, Lisboa, Portugal

ON THE EVALUATION OF LARGE EDDY SIMULATION OF A WIND-TURBINE ARRAY BOUNDARY LAYER

D. FOLCH, F.X. TRIAS AND A. OLIVA

Heat and Mass Transfer Technological Center, Technical University of Catalonia
C/Colom 11, 08222 Terrassa (Barcelona)
david.folch@upc.edu, francesc.xavier.trias@upc.edu, asensio.oliva@upc.edu
http://www.cttc.upc.edu/

Key words: LES, S3PQR models, boundary layer, wind turbine

Summary. Direct numerical simulations of the incompressible Navier-Stokes equations at higher Reynolds numbers are not yet feasible, so dynamically less complex mathematical formulations such as Large Eddy Simulation (LES) have been developed. Over the years, there has been a cumulative improvement in the proposal and design of the models. New ones (namely S3PQR) have been prescribed using the first three principal invariants of the symmetric tensor $\mathsf{G}\mathsf{G}^T$, where $\mathsf{G} \equiv \nabla\overline{\boldsymbol{u}}$ is the gradient of the resolved velocity, with excellent results in the channel flow and homogeneous isotropic turbulence cases.

Recently, these and other LES models have also been applied and compared on the free boundary layer and on a fully developed boundary layer wind farm, using a simplified model of a wind turbine. The S3PQR models have shown outstanding performance.

To ensure complete validation of the S3PQR models, in this work, we run several tests changing the parameters of the algorithm, from coarser to finer resolution. Then, we compare the results with those from a direct numerical simulation. To give a broad view, we test the boundary layer case and a fully developed wind farm.

1 INTRODUCTION

The incompressible Navier-Stokes equations are the mathematical framework when dealing with turbulent flows. However, at large Reynolds numbers where multiple relevant flow scales exist, direct numerical simulation (DNS) becomes unfeasible due to its high resource demands. The Large Eddy Simulation (LES) equations stem from applying a spatial filter to the incompressible Navier-Stokes equations:

$$\begin{aligned} \partial_t\overline{\boldsymbol{u}} + C(\overline{\boldsymbol{u}},\overline{\boldsymbol{u}}) &= D(\overline{\boldsymbol{u}}) - \nabla p - \nabla\cdot\tau(\overline{\boldsymbol{u}}); \\ \nabla\cdot\overline{\boldsymbol{u}} &= 0 \end{aligned} \tag{1}$$

where $\overline{\boldsymbol{u}}$ is the filtered velocity, $C(\overline{\boldsymbol{u}},\overline{\boldsymbol{u}})$ and $D(\overline{\boldsymbol{u}})$ stand for the convective and diffusive terms respectively, p is the pressure, and $\tau(\overline{\boldsymbol{u}})$ is the subgrid stress (SGS) tensor that approximates the effect of the unresolved scales.

This equation needs a closure model to be numerically solved. The LES closure for the eddy-viscosity models is of the type $\tau(\overline{\boldsymbol{u}}) \approx -2\nu_e S(\overline{\boldsymbol{u}})$ where $S(\overline{\boldsymbol{u}}) = 1/2(\nabla\overline{\boldsymbol{u}} + \nabla\overline{\boldsymbol{u}}^T)$ is the rate-of-strain tensor. We must define an eddy viscosity: $\nu_e = (C_m\Delta)^2 D_m(\overline{\boldsymbol{u}})$ where C_m is the model constant, Δ is the subgrid characteristic length [1], and $D_m(\overline{\boldsymbol{u}})$ is the differential operator with units of frequency associated with the model [2].

2 SHORT REVIEW OF S3PQR THEORY

S3PQR are a type of LES models. For a complete description of these models see [3]. To summarize some ideas: besides the trace ($P_{\mathsf{G}} = Tr(\mathsf{G}) = \nabla \cdot \overline{\boldsymbol{u}} = 0$), five mathematical invariants can be calculated from the gradient tensor $\mathsf{G} \equiv \nabla \overline{\boldsymbol{u}}$, namely:

$$\{Q_{\mathsf{G}}, R_{\mathsf{G}}, Q_{\mathsf{S}}, R_{\mathsf{S}}, V_{\mathsf{G}}^2\}$$

For this second-order tensor G, they are defined as [3]

$$\begin{aligned} Q_{\mathsf{G}} &= (1/2)(tr^2(\mathsf{G}) - tr(\mathsf{G}^2)) \\ R_{\mathsf{G}} &= det(\mathsf{G}) \\ Q_{\mathsf{S}} &= (1/2)(tr^2(\mathsf{S}) - tr(\mathsf{S}^2)) \\ R_{\mathsf{S}} &= det(\mathsf{S}) \\ V_{\mathsf{G}}^2 &= 4(tr(S^2\Omega^2) - 2Q_S Q_\Omega) \end{aligned} \tag{2}$$

where $\mathsf{S} = 1/2(\mathsf{G} + \mathsf{G}^T)$ and $\Omega = 1/2(\mathsf{G} - \mathsf{G}^T)$ are the symmetric and the skew-symmetric parts of the gradient tensor, respectively. For any incompressible flow, any invariant can be written as a function of them.

The S3PQR models [3] involve the three principal invariants of the symmetric tensor $\mathsf{G}\mathsf{G}^T$, which is the leading term in the Taylor-series expansion of the SGS tensor [4],

$$\tau(\overline{\boldsymbol{u}}) = \frac{\Delta^2}{12}\mathsf{G}\mathsf{G}^T + \mathcal{O}(\Delta^4) \tag{3}$$

These invariants are directly related to the previous ones

$$\begin{aligned} P_{\mathsf{G}\mathsf{G}^T} &= tr(\mathsf{G}\mathsf{G}^T) = 2(Q_\Omega - Q_{\mathsf{S}}) \\ Q_{\mathsf{G}\mathsf{G}^T} &= 2(Q_\Omega - Q_{\mathsf{S}})^2 - Q_{\mathsf{G}}^2 + 4tr(\mathsf{S}^2\Omega^2) \\ R_{\mathsf{G}\mathsf{G}^T} &= det(\mathsf{G}\mathsf{G}^T) = det(\mathsf{G})det(\mathsf{G}^T) = R_{\mathsf{G}}^2 \end{aligned} \tag{4}$$

So now one can construct new models [3]:

$$\nu_e = (C_{s3pqr}\Delta)^2 P_{\mathsf{G}\mathsf{G}^T}^p Q_{\mathsf{G}\mathsf{G}^T}^q R_{\mathsf{G}\mathsf{G}^T}^r \tag{5}$$

If we restrict them to solutions involving only two invariants, then we have for example:

$$\nu_e^{S3PR} = (C_{s3pr}\Delta)^2 P_{\mathsf{G}\mathsf{G}^T}^{-1} R_{\mathsf{G}\mathsf{G}^T}^{1/2} \tag{6}$$

for the S3PR model.

Finally, there are two ways to determine the model constant for the S3PQR models:

1. Imposing numerical stability and less or equal dissipation than Vreman's model [5]. Then
$$C_{s3pq} = C_{s3pr} = C_{s3qr} = \sqrt{3}C_{Vr} \approx 0.458$$
2. Granting that the averaged dissipation of the models is equal to that of the Smagorinsky model. Then
$$C_{s3pq} = 0.572,\ C_{s3pr} = 0.709,\ C_{s3qr} = 0.762$$

Further characteristics of these LES S3PQR models are positiveness, locality, Galilean invariance, and proper near-wall behaviour [6] ($\mathcal{O}(y^3)$ dependence on normal direction).

Throughout this work, the computations have been done with the S3PR type 2 constant. There are previous computations and comparisons between models like those of Smagorinsky, Verstappen [7], WALE [8], Vreman [5], and all the S3PQR, in [9]. All of them shared algorithm characteristics such as: $Re_{\delta^*} = 1000$, where δ^* is the displacement thickness; growing terms (equivalent as a forcing term) $GT(\overline{\boldsymbol{u}}, \overline{U})$, from [10]; and zero mean pressure gradient case. The mesh size for all was $N_x \times N_y \times N_z = 32 \times 64 \times 32$ for streamwise, normal, and spanwise directions, enough to yield good results in the S3PQR cases. In this previous work, S3PR stood as slightly the best of all of them.

3 SEMI-IMPLICIT PROCEDURE

Spectral methods have demonstrated a remarkable ability to accurately calculate derivatives, making them a valuable tool in scenarios where periodic conditions are applicable[11]. Nevertheless, these methods necessitate strict periodicity, which is not characteristic of a developing boundary layer, posing a significant challenge in their application to such computations. Then it is necessary to take a different approach to justify these periodic conditions, such as the method proposed by [10, 12], which includes normal coordinate similarity transformations, growing terms $GT(\overline{\boldsymbol{u}}, \overline{U})$, and several other assumptions.

We use a pseudo-spectral method [13], with a Fourier expansion in the streamwise and spanwise directions, and Chebyshev expansion for the normal one. It applies the 3/2 rule de-aliasing technique. The computation code is based on MPI parallelization.

Although Chebyshev polynomials are useful when dealing with Dirichlet and Newman boundary conditions, they suffer from a main drawback: the CFL condition leads to time-step of order $O(1/N^2)$ for the convective term and $O(1/N^4)$ for the diffusive term [14]. Then, fine mesh computations are not feasible using fully explicit methods. It is necessary to resort to implicit schemes. The solution adopted here is to compute explicitly the convective term and implicitly the diffusive term.

The S3PQR LES methods yield non-uniform (and non-constant) eddy viscosity. For the implicit diffusive term, at each step, we should compute a triple convolution sum that goes as this eddy viscosity ν_e multiplied by the scaling factor of the semi-infinite domain multiplied by the Chebyshev derivative coefficients. It is again unfeasible at every step. A general class of two-step methods are usually described by a parameter θ such as for the diffusive term [14]:

$$D(u) = \nabla \cdot [(\nu + \nu_e)(\theta(\nabla u^{n+1} + (\nabla u^{n+1})^T) + (1-\theta)(\nabla u^n + (\nabla u^n)^T))] \tag{7}$$

where ν is the physical viscosity of the fluid.

We can then make a slight modification:

$$D(u) = (0.5\nu)\nabla^2 u^{n+1} + \nabla \cdot ((0.5\nu + \nu_e)(\nabla u^n + (\nabla u^n)^T)) \tag{8}$$

With this rearrangement:

1. We calculate the matrix operator **only once** at the beginning with ν uniform and constant.
2. We loose time-step requirements: from $O(1/N^4)$ to $O(1/N^2)$, approximately.

4 NUMERICAL TEST

For the assesment of the models, we will test the NO-MODEL vs S3PR LES model. The mesh sizes $N_x \times N_y \times N_z$ used in these computations are $32 \times 64 \times 32 \rightarrow 64 \times 64 \times 64 \rightarrow 96 \times 96 \times 96 \rightarrow$

$128 \times 128 \times 128$, where x, y, and z, are the streamwise, wall-normal and spanwise directions. The Reynolds number is again fixed along the simulation to $Re_{\delta^*} = 1000$, to compare with the previous results [9].

For the case 128^3, $\Delta x^+ \approx 20$, $\Delta z^+ \approx 6.7$ in wall units, and for the wall-normal, there are 11 points within 9 wall units of the wall. These are similar values to those of the Spalart et al. DNS simulation [12].

4.1 Boundary layer

First, we deal with the free boundary layer (BL) cases. As we have said before, the structure of the algorithm for a BL is based on the method proposed by [10]. To evaluate the performance of the methods, we focus on the evolution of friction velocity. As you can see in Table 1, we can

Mesh size	NO-MODEL	S3PR
$32 \times 64 \times 32$	0.056	0.049
64^3	0.051	0.048
96^3	0.049	0.048
128^3	0.049	0.048
Sp-Le DNS	**0.049**	

Table 1: Friction velocity values. Reference: Sp-Le DNS, with $264 \times 60 \times 170$ [10] or $256 \times 64 \times 192$ [12]

appreciate two slightly different behaviors. For the NO-MODEL algorithm, using a coarse mesh, we obtain a result way off the DNS value. As we refine the mesh, we approach the reference value, as expected. On the other hand, for the S3PR model, we directly obtain the desired value, right from the coarse mesh, with a consistent evolution.

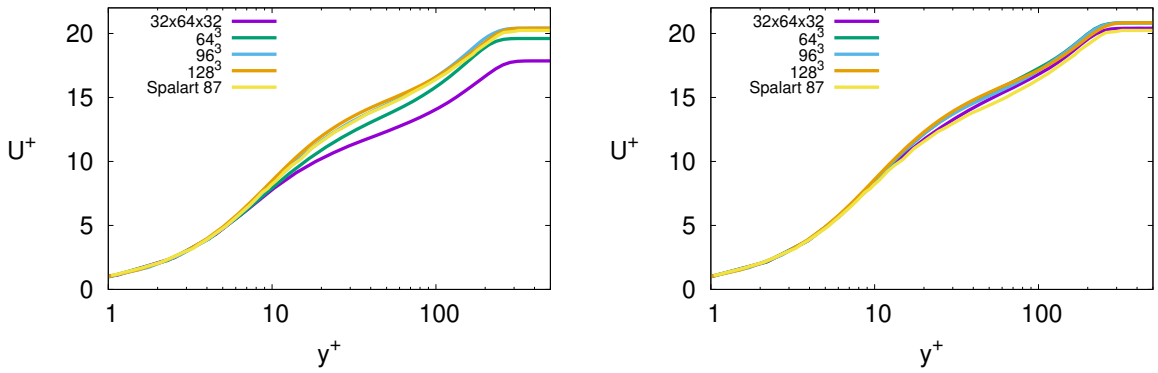

Figure 1: BL average streamwise velocity profile. Mesh size $N_x \times N_y \times N_z$. Left: NO-MODEL. Right: S3PR model. Reference: Spalart 87 [10], with $264 \times 60 \times 170$

In Figures 1 and 2, we plot the average streamwise velocity profiles. The same general behavior is present. The NO-MODEL starts far from the reference profile, in the case of the

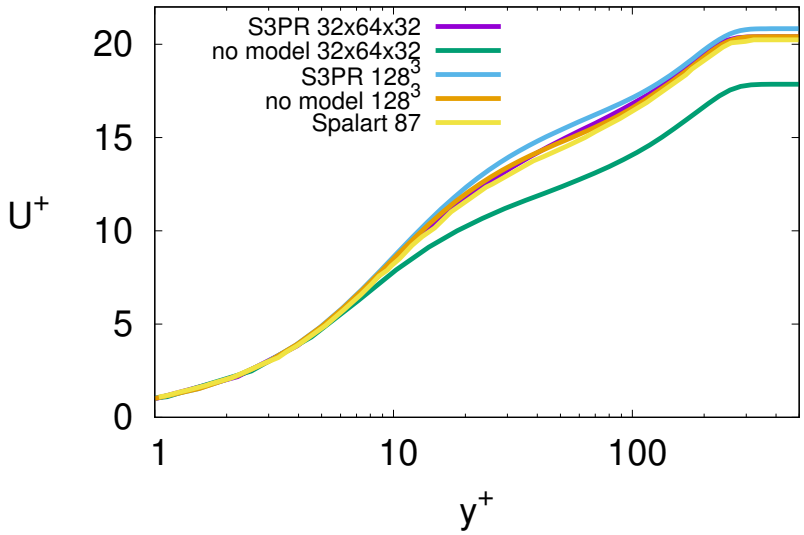

Figure 2: BL average streamwise velocity profile. Mesh size $N_x \times N_y \times N_z$. Comparison between NO-MODEL and S3PR model. Reference: Spalart 87 [10], with $264 \times 60 \times 170$

very coarse mesh, and then approaches the expected profile for the finer meshes. For the S3PR method, we already observe rather good results, even for the coarse mesh. Actually, it is exactly the desired aim of the LES models like this S3PR model.

4.2 Wind farm

For the wind farm simulations, we will follow the same layout and assumptions as the BL plus a disk actuator for every wind turbine. The specifications of these disk actuators follow from [15], and they can be straightforwardly applied to our algorithm, see Figure 3.

As with the BL, we plot the streamwise velocity profile. Unfortunately, we have no reference to compare to, so we must rely on the general trend of the calculations to see whether they converge to the same final values. In Figures 4 and 5 we show the results.

As expected, the general trend is the same as that of the BL with slight differences. Both the NO-MODEL and the S3PR approach an asymptotic profile that is roughly the same. For the coarsest mesh, the NO-MODEL is clearly worse than the S3PR. Regarding the LES model, the convergence to the final values is faster than the NO-MODEL. It seems that with a finer resolution mesh, like 256^3 or higher, the small divergences seen at a 128^3 mesh should vanish.

As shown in [15], we can expect two well-defined log laws along the vertical velocity profile, represented as two minima when plotting the streamwise velocity derivative, $y^+ du^+/dy^+$ vs. y^+. See Figures 6 and 7.

Although they are noisy and sensitive graphs, the previously observed general trend can be seen in Figures 6 and 7. It should be noted that there is not this expected second minima for the NO-MODEL with coarse meshes, whereas for the S3PR it appears right from the beginning.

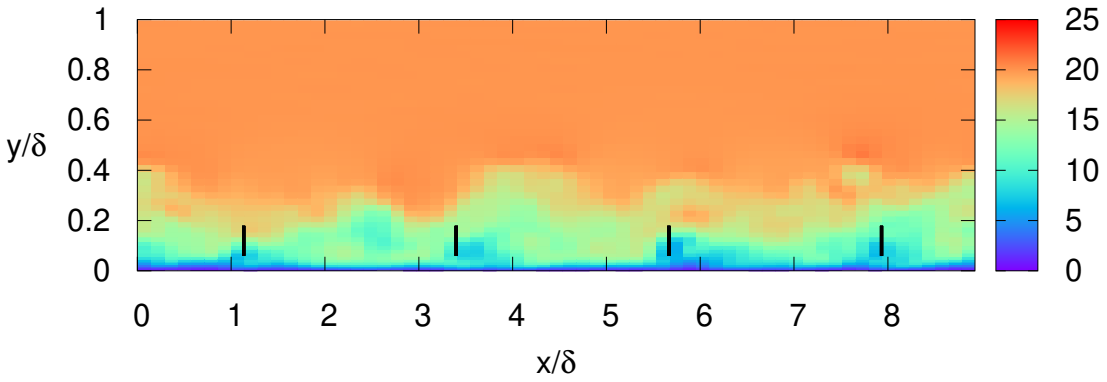

Figure 3: Wind farm. S3PR model. Normalized instantaneous streamwise velocity u^+ at a sample time. Disk actuators depicted as black solid lines. δ stands as the BL thickness. Mesh size: $64 \times 64 \times 64$.

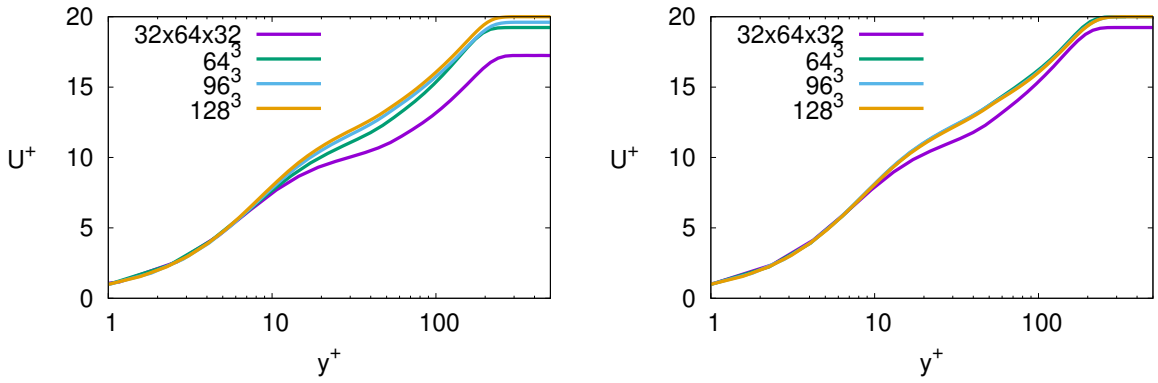

Figure 4: Wind farm average streamwise velocity profile. Left: NO-MODEL. Right: S3PR model. Mesh size $N_x \times N_y \times N_z$

5 CONCLUSIONS

We have evaluated the performance of the S3PR LES model through different resolution meshes and compared it with the NO-MODEL behavior.

The NO-MODEL simulation consistently approaches an asymptotic profile with a finer resolution. On the other hand, the S3PR method gives the same asymptotic profile, even for coarse resolution. In the case of the BL, it is seen for both methods, whereas for the wind farm a slightly higher resolution mesh seems to be needed.

The observed asymptotic profile matches that of the reference, in the case of the BL. The performance of the two models is then what was expected, and about the S3PR model, desired. Moreover, the specifically designed semi-implicit algorithm allows for these higher-resolution computations.

Once the validity and adaptability of these S3PQR models have been shown, they could

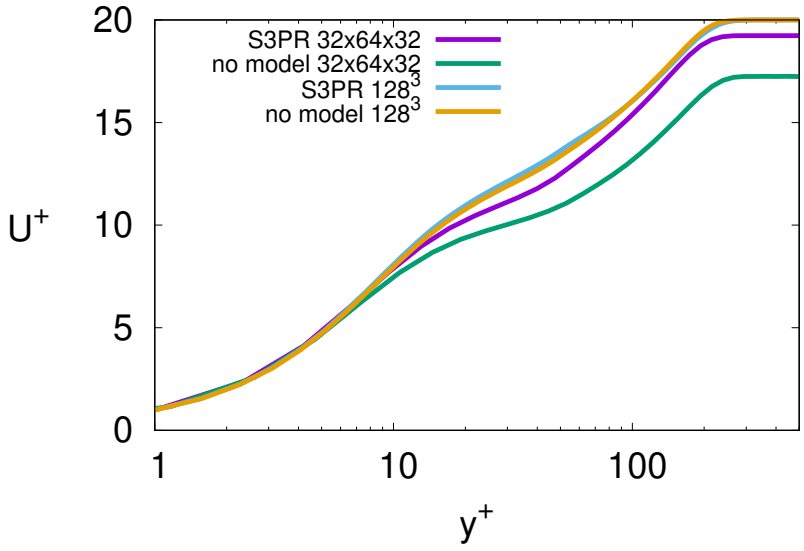

Figure 5: Wind farm average streamwise velocity profile. Mesh size $N_x \times N_y \times N_z$. Comparison between NO-MODEL and S3PR model

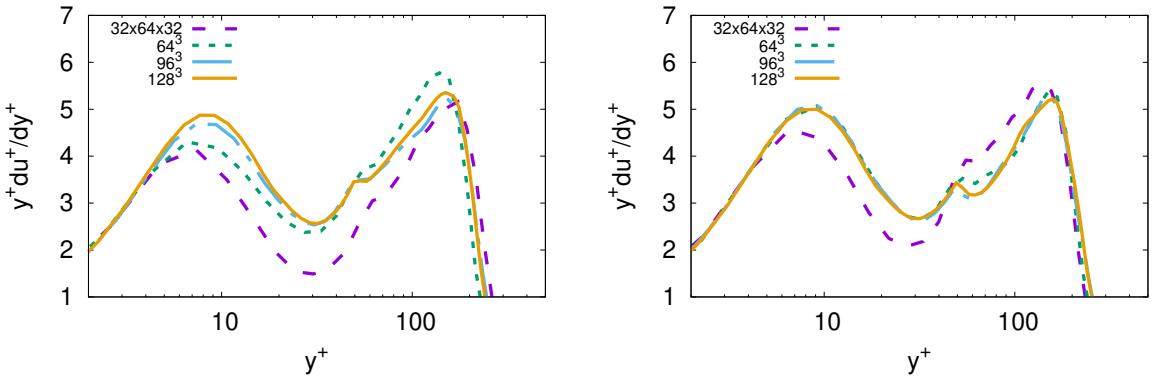

Figure 6: Wind farm average streamwise velocity derivative. Left: NO-MODEL. Right: S3PR model. Mesh size $N_x \times N_y \times N_z$

be applied to real-life scenarios, including different engineering boundary layers, wind farms, dispersion of pollutants, etc. Despite the power of the spectral methods, finally their CFL time-step constrain would be prohibitive, so we should resort to non-spectral methods.

Acknowledgements. This work is supported by SIMEX project (PID2022-142174OB-I00) of *Ministerio de Ciencia e Innovación* and the RETOtwin project (PDC2021-120970-I00) of *Ministerio de Economía y Competividad*, Spain. The authors thankfully acknowledge these institutions.

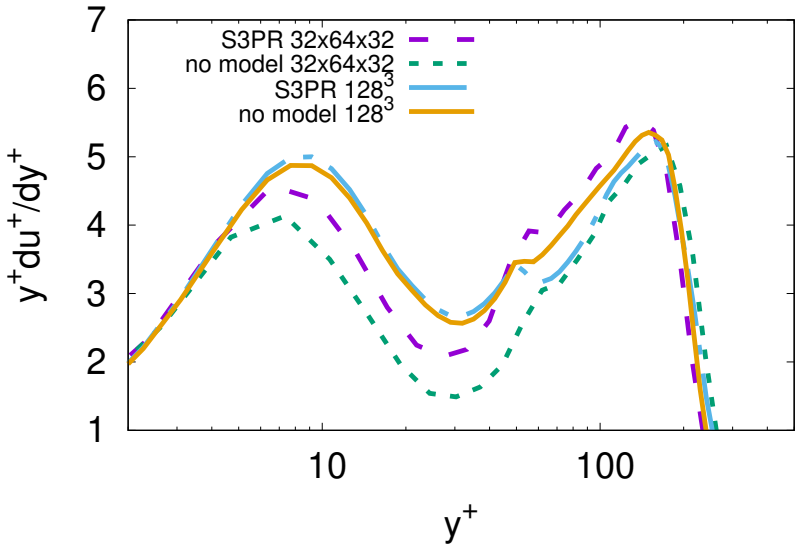

Figure 7: Wind farm. Average streamwise velocity derivative. Mesh size $N_x \times N_y \times N_z$. Comparison between NO-MODEL and S3PR model

REFERENCES

[1] F. X. Trias, A. Gorobets, M. H. Silvis, R. W. C. P. Verstappen, and A. Oliva, "A new subgrid characteristic length for turbulence simulations on anisotropic grids," *Physics of Fluids*, vol. 29, p. 115109, 2017.

[2] F. Nicoud, H. B. Toda, O. Cabrit, S. Bose, and J. Lee, "Using singular values to build a subgrid-scale model for large eddy simulations," *Physics of Fluids*, vol. 23, no. 8, p. 085106, 2011.

[3] F. X. Trias, D. Folch, A. Gorobets, and A. Oliva, "Building proper invariants for eddy-viscosity subgrid-scale models," *Physics of Fluids*, vol. 27, no. 6, p. 065103, 2015.

[4] R. A. Clark, J. H. Ferziger, and W. C. Reynolds, "Evaluation of subgrid-scale models using an accurately simulated turbulent flow," *Journal Fluid Mechanics*, vol. 91, pp. 1–16, 1979.

[5] A. W. Vreman, "An eddy-viscosity subgrid-scale model for turbulent shear flow: Algebraic theory and applications," *Physics of Fluids*, vol. 16, no. 10, pp. 3670–3681, 2004.

[6] D. R. Chapman and G. D. Kuhn, "The limiting behaviour of turbulence near a wall," *Journal of Fluid Mechanics*, vol. 170, pp. 265–292, 1986.

[7] R. Verstappen, "When does eddy viscosity damp subfilter scales sufficiently?," *Journal of Scientific Computing*, vol. 49, no. 1, pp. 94–110, 2011.

[8] F. Nicoud and F. Ducros, "Subgrid-scale stress modelling based on the square of the velocity gradient tensor," *Flow, Turbulence and Combustion*, vol. 62, no. 3, pp. 183–200, 1999.

[9] D. Folch, F. X. Trias, and A. Oliva, "Assessment of LES models for a fully developed windturbine array boundary layer," *10th International Symposium on Turbulence, Heat and Mass Transfer, THMT-23, Rome, Italy, 11-15 September 2023*, 2023.

[10] P. Spalart and A. Leonard, *Direct Numerical Simulation of Equilibrium Turbulent Boundary Layers*. Berlin: Springer-Verlag, 1987.

[11] J. P. Boyd, *Chebyshev and Fourier Spectral Methods*. Dover Publications, Inc., 2001.

[12] P. Spalart, "Direct simulation of a turbulent boundary layer up to $R_\theta = 1410$," *Journal of Fluid Mechanics*, vol. 187, pp. 61–98, 1988.

[13] F. X. Trias, D. Folch, A. Gorobets, and A. Oliva, "Spectrally-consistent regularization of Navier-Stokes equations," *Journal of Scientific Computing*, vol. 79, pp. 992–1014, 2019.

[14] R. Peyret, *Spectral Methods for Incompressible Viscous Flow*. Springer New York, NY, 2013.

[15] M. Calaf, C. Meneveau, and J. Meyers, "Large eddy simulation study of fully developed wind-turbine array boundary layers," *Physics of Fluids*, vol. 22, p. 015110, 2010.